Soft Matter RSCPublishing

COMMUNICATION

Mapping surface tension induced meniscus with application to tensiometry and refractometry

Cite this: DOI: 10.1039/x0xx00000x

Avanish Mishra,[a] Varun Kulkarni[b] Jian-Wei Khor [a] and Steve Wereley*[a]

Received 00th January 2015, Accepted 00th January 2015

DOI: 10.1039/x0xx00000x

www.rsc.org/

In this work, we discuss an optical method for measuring surface tension induced menisci. The principle of measurement is based upon the change in background pattern produced by the curvature of the meniscus acting as a lens. We measure meniscus profile over an inclined glass plate and utilize the measured meniscus for estimation of surface tension and refractive index.

The phenomenon of heavier entities floating at the liquid-gas interface is an intriguing occurrence in nature. In such scenarios, liquid-gas interface deforms and the weight of object is balanced by the surface tension force. The extent of liquid surface deformation, also known as the meniscus, gives us the magnitude of surface tension force at play. Analysing the meniscus is key to unravelling the underlying physical mechanisms of capillary interactions in agglomerating particles on a liquid surface during self-assembly[1–3] and locomotion of arthropods such as water striders[4]. In such cases, meniscus may not be axisymmetric and may vary with time. Additionally and more importantly, it may be too small to be captured accurately using conventional side view imaging. A technique that can accurately perform whole field, microscale, three-dimensional (3D) meniscus measurement would be of great benefit to researchers in this area. Conventional methods for measuring the topography of free surfaces rely on laser beam refraction[5] which can achieve only point or line measurements implying that whole field information cannot be obtained[6]. Moreover, these methods often require a complex and labour intensive optical setup. Researchers have also used collimated light to obtain the whole field surface deformation[7]. Although this approach is simpler, these methods still require a complex optical setup due to the use of collimating optics. Expanding upon the work of Moisy et al.[8], we discuss a background (synthetic Schlieren) imaging method for measuring 3D profile of surface tension induced meniscus. Synthetic Schlieren imaging utilizes scattered light, considerably simplifying the experimental setup and procedure[8]. Until now, Schlieren imaging has not been used for measuring surface tension induced meniscus. In this work, we set out to accomplish two key objectives, 1) demonstrate the accuracy of Schlieren imaging for measuring surface tension induced deformations, and 2) to develop a tensiometer based on it. To establish accuracy of Schlieren imaging, we measure meniscus profile over an inclined glass plate as an exact analytical solution is known for this case. We then utilize the measured meniscus profile for estimation of surface tension and refractive index. Successful measurement of surface tension of various test liquids proves that a surface tension induced meniscus can be measured by Schlieren imaging and, as will be shown later, it can also be used for measurement of liquid refractive index. At present the common approaches for measuring surface tension are the Wilhelmy plate, du Noüy ring, pendant or sessile drop method and bubble pressure method. A comprehensive summary of these techniques can be found in Drelich[9]. Pendant and sessile drop methods are of particular interest and superior to others in several ways. However, the side view imaging employed in these methods provides only axisymmetric information about drops[10]. Thus, the sessile drop approach is not suitable for inhomogeneous substrates or when the drop shape is not axisymmetric. The pendant drop method is also difficult to apply to low interfacial tension (<0.1 mN/m) fluids due to increased difficulty in retaining the drop on the needle tip[9]. The experimental scheme being proposed in this work will provide 3D profile of meniscus over the whole contact line, irrespective of low surface tension as background imaging is highly sensitive to surface gradient.

The experimental setup is shown in Fig. 1. For measuring 3D profile of meniscus, we adopt and expand upon the free surface synthetic Schlieren method[8]. A random dot pattern is placed below the liquid vessel. This background pattern is then imaged from above by a camera. Two images are recorded, one before the glass plate is inserted, when interface is planar and one after the insertion of the inclined glass plate when meniscus is present. Due to the curvature of the meniscus behaving like a lens, the background pattern appears displaced between the two images. The apparent displacement field between the two images is determined by digital cross correlation[11]. Based on the geometric optics ray tracing approach, the dot pattern displacement at any point can be related to the meniscus gradient which can be numerically integrated to obtain the meniscus profile[8]. The experimentally determined meniscus profile is then fitted to the theoretical equation of the meniscus over an inclined plate, which yields surface tension and contact angle as fit parameters. Moreover, using the same procedure we can also obtain the value of the refractive index of liquid. At locations far away from the contact line, surface tension induced deformation is negligible and the displacement of the background pattern is purely due to refraction at the inclined plate/liquid and liquid/air interfaces. We utilize this information to estimate the refractive index of the liquid. Thus, experimental setup shown in Fig. 1 can not only be used to measure the meniscus profile but it can also be used for simultaneous tensiometry and refractometry of liquids.

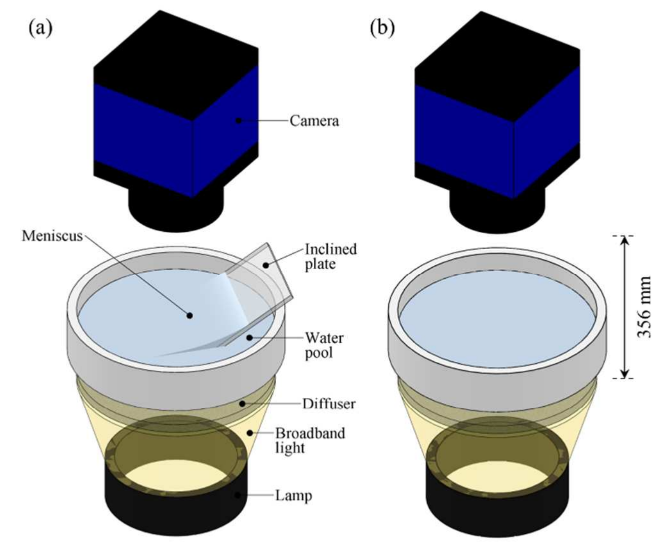

Fig. 1 Experimental setup consists of an imaging camera, a liquid vessel, a flat plate, a background pattern and the broadband illumination. (a) Imaging of background pattern through meniscus and (b) imaging of background pattern through planar surface. As part of the experimental procedure, the background pattern is imaged through the planar and deformed interface. Displacement of the pattern between two images is related to surface gradient to obtain the meniscus profile.

The following sections begin with a description of the underlying optics and the calculations involved. We show that the displacement field is directly proportional to the surface gradient of the meniscus as long as a correction factor for the inclined glass plate is included. Next the details of the theoretical model of the meniscus in contact with an inclined plate are presented. Then the fit parameters for surface tension and contact angle are extracted by comparing the measured meniscus profile with the mathematical model for the meniscus. Finally, to conclude, a comparison of the experimental measurements with literature data and pendant drop technique is provided.

In order to determine the relationship between the dot pattern displacement field and the surface gradient, first we have to look at the case of a planar liquid surface as depicted in Fig. 2. We consider the case where random dot pattern is located at $z=0$ and the camera, C is located at a height H from the pattern. h_p is the height of the liquid surface, n is the refractive index of gas while n' is the refractive index of liquid. Rays emanating from point M on the pattern will undergo refraction at the free surface and appear to come from point M′ on the pattern plane. The incidence plane COP is defined by refracted ray CI and the normal unit vector $\hat{\boldsymbol{n}}$. It is perpendicular to the $z=0$ plane. As a result, apparent displacement MM′ takes place in the radial direction $\hat{\boldsymbol{r}}$. Looking at triangles Δ IKM′ and Δ IKM and assuming that the camera to pattern distance H is large enough that paraxial approximation is reasonable, we get

$$\mathbf{MM'} = \mathbf{KM'} - \mathbf{KM} \quad (1)$$

$$\mathbf{MM'} = h_p\left(\tan i - \tan i'\right)\hat{\boldsymbol{r}} = h_p\left(i - i'\right)\hat{\boldsymbol{r}} = h_p i\left(1 - \frac{i'}{i}\right)\hat{\boldsymbol{r}} \quad (2)$$

By applying the Snell-Descartes law at the point of incidence I, subject to the paraxial approximation, we get

$$\frac{n}{n'} = \frac{i'}{i} \quad (3)$$

Replacing i'/i in Equation 2, we get

$$\mathbf{MM'} = \alpha h_p i\hat{\boldsymbol{r}}\text{, where } \alpha = 1 - n/n' \quad (4)$$

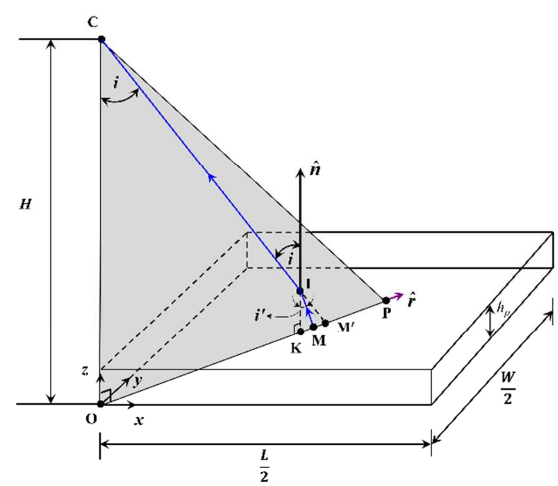

Fig. 2 Refraction optics at the plane liquid/air interface. A point M on the background pattern appears to be located at M′. The Blue line indicates a ray from point M to camera C and I is the point of intersection of the ray with the interface. L and W denote the length and the breadth of the field of view while $\hat{\boldsymbol{n}}$ is the surface normal unit vector at point I.

Next we consider the case of inclined glass plate with meniscus, as depicted in Fig. 3 which shows ray geometry in the plane of incidence. The primary objective of the technique is to measure $\boldsymbol{\delta r}$, which is the optical displacement of the point M′ to M″ due to refraction at the liquid/glass interfaces and the liquid/air interface (Fig. 4). We assume that the height variation of the meniscus is very small as compared to the pattern to surface distance h_p. We also assume a small slope approximation, which means that the surface slope θ is very small. In our experimental configuration we have a flat plate immersed in the liquid which increases the displacement of the point M to M^{o}. The displacement MM^{o} must be accounted to measure the surface gradient accurately. We have developed an analytical expression for magnitude of MM^{o} (see Supporting Information for derivation),

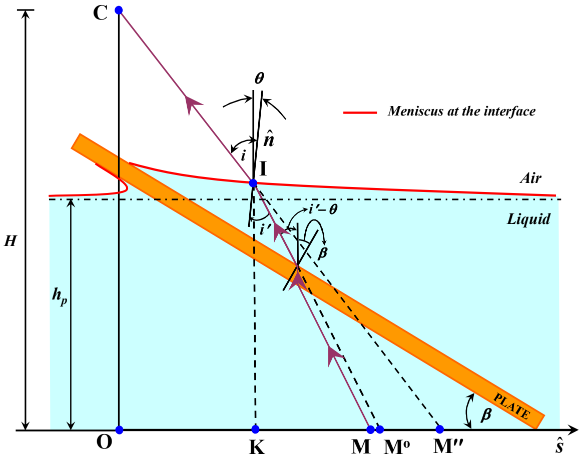

Fig. 3 Geometric ray tracing optics at the liquid/air interface and liquid/glass interfaces showing a point on the speckled pattern, M and its corresponding displacement M$^{\circ}$ and M″.

$$\mathrm{MM}^{\circ} = \frac{l}{\cos\phi}\sin\left(\beta-\phi\right), \text{ where } \phi = \sin^{-1}\left(\frac{n'\sin\beta}{n_g}\right) \tag{5}$$

In the above expression, l is the thickness of the flat plate in the incidence plane, n_g is the refractive index of glass and β is the angle of the inclination of the plate. In order to understand relationship between surface gradient and displacement field, we now focus our attention to the refraction at the meniscus. Let the surface be represented by $z = h(x,y)$ whose normal, $\hat{\boldsymbol{n}}$ is given by,

$$\hat{\boldsymbol{n}} = \frac{\hat{z}-\nabla h}{\sqrt{1+\left(\nabla h\right)^{2}}} \tag{6}$$

Here, ∇h is the gradient of the meniscus. Assuming the weak slope approximation ($\nabla h \ll 1$) we get,

$$\nabla h = \hat{z} - \hat{\boldsymbol{n}} \tag{7}$$

Next, we define $\hat{\boldsymbol{s}}$ as the unit vector along which displacement from M to M″ takes place. It is lying on the incidence plane CAM″ (Fig. 4). In terms of variables defined in Fig. 3 and Fig. 4 this can be written as

$$\hat{\boldsymbol{s}} = \frac{\mathbf{M^{\circ}M''}}{\left|\mathbf{M^{\circ}M''}\right|} \tag{8}$$

Using the weak slope and paraxial approximations, we can show that (see Supporting Information for derivation)

$$\hat{\boldsymbol{n}} = i\hat{\boldsymbol{s}} - \frac{\mathbf{CM''}}{\left|\mathbf{CM''}\right|} \tag{9}$$

It is worthwhile to note that, $\mathbf{CM''} = \mathbf{CO} + \mathbf{OM''}$ and $\left|\mathbf{CM''}\right| \approx H$, the distance of the camera from the pattern. Combining eqn (7) and eqn (9) together, we get an expression for ∇h

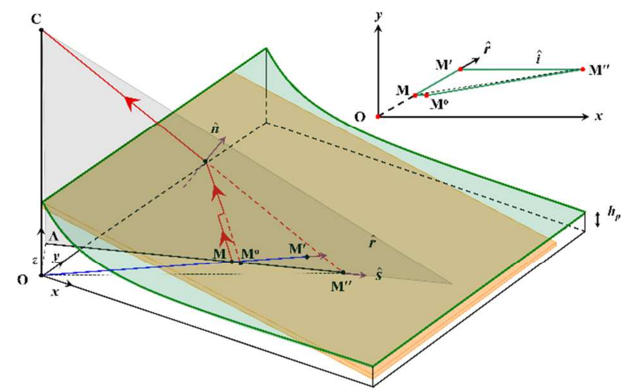

Fig. 4: Three-dimensional ray geometry for a deformed interface. The incidence plane CAM″ is defined by the object point M, the camera C, and the unit normal vector $\hat{\boldsymbol{n}}$ at point I. This plane is not vertical in general.

$$\nabla h = \hat{z} - i\hat{s} + \left(\frac{\mathbf{CO}+\mathbf{OM''}}{H}\right) = \frac{\mathbf{OM''}}{H} - i\hat{s} \tag{10}$$

Considering Δ IKM and Δ IKM″ in the incidence plane as shown in Fig. 3, it can be proved that (see Supporting Information for derivation),

$$\mathbf{M^{\circ}M''} = \mathbf{KM''} - \mathbf{KM^{\circ}} = \alpha h_p i\hat{\mathbf{s}} \tag{11}$$

Equation 11 transforms eqn (10) to

$$\nabla h = \frac{\mathbf{OM''}}{H} - i\frac{\mathbf{M^{\circ}M''}}{\alpha h_p i} = \frac{\mathbf{OM''}}{H} - \frac{\mathbf{M^{\circ}M''}}{\alpha h_p} \tag{12}$$

We know that $\mathbf{MM''}$ is equal to $\mathbf{MM'} + \boldsymbol{\delta r}$, which leads to

$$\mathbf{M^{\circ}M''} = \mathbf{MM''} - \mathbf{MM^{\circ}} = \mathbf{MM'} + \boldsymbol{\delta r} - \mathbf{MM^{\circ}} \tag{13}$$

$$\mathbf{OM''} = \mathbf{OM'} + \boldsymbol{\delta r} \tag{14}$$

$$\nabla h = \frac{\mathbf{OM'}+\boldsymbol{\delta r}}{H} - \frac{\mathbf{MM'}+\boldsymbol{\delta r}-\mathbf{MM^{\circ}}}{\alpha h_p} \tag{15}$$

From eqn (4) and Fig. 2, it can be proved that

$$\frac{\mathbf{OM'}}{H} = \frac{\mathbf{MM'}}{\alpha h_p} = i \tag{16}$$

Combining eqn (15) and eqn (16), we get

$$\nabla h = \frac{\boldsymbol{\delta r}}{H} - \frac{\boldsymbol{\delta r}-\mathbf{MM^{\circ}}}{\alpha h_p} \tag{17}$$

$\frac{\boldsymbol{\delta r}}{H}$ is negligible in comparison to $\frac{\boldsymbol{\delta r}-\mathbf{MM^{\circ}}}{\alpha h_p}$ as $H >> \alpha h_p$

$$\nabla h = -\frac{\delta \boldsymbol{r} - \mathbf{MM}^{o}}{\alpha h_p} \tag{18}$$

Equation (18) shows that the surface gradient is proportional to displacement field as long as displacement $\mathbf{MM^o}$ from inclined plate is taken in to consideration. We have already derived an expression for magnitude of $\mathbf{MM^o}$ in the form of eqn (5).

To obtain a theoretical expression for the meniscus, the Young-Laplace equation is solved in Cartesian coordinates (see Supporting Information for derivation). The expression for the meniscus height (h) as a function of the distance (x) is given by

$$\frac{h}{l_c} = tan(\alpha)e^{-x/l_c} \tag{19}$$

In this expression, $l_c\,(=\sqrt{\sigma / \rho g}\,)$ is the capillary length and $\alpha = \beta - \theta_c$, where θ_c is the contact angle. σ and ρ are surface tension and density of liquid, respectively and g is the acceleration due to gravity.

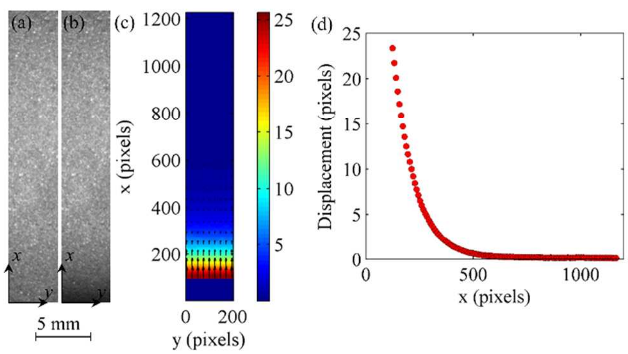

Fig. 5 (a) image of the background pattern with plane dodecane surface, (b) image of the background pattern with meniscus, (c) computed displacement field, and (d) displacement magnitude $M'M''$ as a function of distance from the inclined plate.

In order to validate the technique, a dodecane-air system was chosen for the experiments. Images were recorded using a Nikon DS-fi1 camera equipped with a 40 mm Micro-Nikkor lens. We utilized a glass diffuser as an inexpensive random dot background pattern. A 0.15 mm thick and 50×75 mm^2 glass plate mounted on a rotation platform stage was used as the inclined flat plate. Fig. 5(a) and 5(b) show images of the background pattern through the plane dodecane surface (Configuration A) and through the inclined plate and meniscus (Configuration B), respectively. The displacement of the dot pattern between the two images can be manually observed. In this work we have used commercial PIV package DaVis 7.2® for the computation of the displacement field[11] (see Supporting Information for discussion on PIV evaluation parameters). Fig. 5(c) shows the computed displacement field. Angle of the inclined plate was set to 13.55˚. In Fig. 5b, meniscus starts at y = 0 line. A small region near the inclined plate could not be imaged due to high surface gradient. This region can be identified by lower intensity values near origin in Fig. 5(b). During the displacement field evaluation, we masked out this region. The lack of data in the starting part of meniscus does not affect results of surface tension or contact angle as the rest of the meniscus profile is available for fitting. Fig. 5(d) shows a plot of the displacement $\boldsymbol{\delta r}$ as a function of the distance from the inclined plate. As shown in eqn (18), the displacement is higher in the region of high surface gradient near the inclined plate and it decays to a finite constant value of 0.11 pixel. This final constant displacement value is due to the inclined plate alone. It can be recognized as $\mathbf{MM^o}$ and theoretically estimated to be 0.11 pixel by eqn (5). Both the experimental and theoretical values of $\mathbf{MM^o}$ are same which validates our analysis. Since we can experimentally measure $\mathbf{MM^o}$, we can rather use eqn (5) for determining the refractive index of the liquid. Therefore, this setup acts both as a refractometer and a tensiometer. It is imperative to note that the displacement produced by 0.15 mm thick glass plate is very small. Therefore, we performed separate experiments with a 0.98 mm thick glass plate inserted at steeper angles for refractive index estimation. For estimating dodecane refractive index, a glass plate was inserted at an angle of 20.30˚. It produces an experimental displacement of 1.11±0.02 pixel which can be easily measured with high accuracy. After performing pixel to mm conversion, this value was substituted in eqn (5) for determining the liquid refractive index. Following this scheme, refractive index of dodecane was ascertained to be 1.421±0.002 which is very close to the reported value of 1.422 in literature[12]. The accuracy of the refractive index results can be further improved by using even a thicker glass plate and by increasing the angle of the inclined plate.

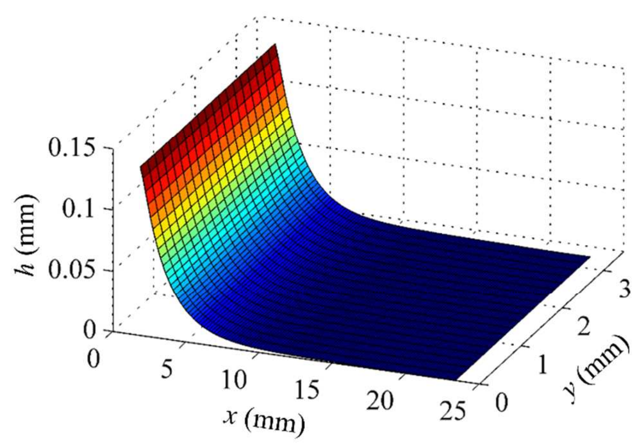

Fig. 6: Three-dimensional (3D) profile of dodecane meniscus on an inclined plate.

For estimating surface tension, $\mathbf{MM^o}$ (0.11 pixel) was subtracted from the original displacement profile. Equation (18) was numerically integrated to obtain the 3D profile of the meniscus as shown in Fig. 6. Figure 7 shows the two-dimensional profile of the dodecane meniscus. The experimentally determined meniscus profile was fitted with eqn (19) to determine the surface tension and contact angle. This experiment was repeated 10 times. The surface tension of dodecane was evaluated to be 25.2±0.4 mN/m which is very close to the value of 25.3 mN/m reported in literature [13]. The contact angle was estimated to be 1.73±0.20˚ which is very close to the value of 1.75±0.06˚ measured by the goniometer. In order to further validate the method, experiments were performed with electronic grade acetone, isopropyl alcohol, and water. Each experiment was repeated ten times. Results are shown in Table 1. It can be clearly observed that the measured values of surface tension and refractive index match the data reported in literature

Table 1: Comparison of surface tension and refractive index obtained from background imaging with the reported data in literature

	Surface Tension (mN/m)			Refractive Index	
	Background Imaging	Pendant Drop Method	Literature	Background Imaging	Literature
Dodecane	25.2±0.4	25.8±2.6	25.3[13]	1.421±0.002	1.422[12]
Acetone	23.3±1.3	23.0±3.3	23.2[12]	1.356±0.001	1.358[12]
Isopropyl Alcohol	22.4±0.5	22.2 ±0.7	21.7[14]	1.374±0.004	1.378[12]
Water	71.6±0.8	71.1±0.6	72.8[14]	1.334±0.001	1.333[12]

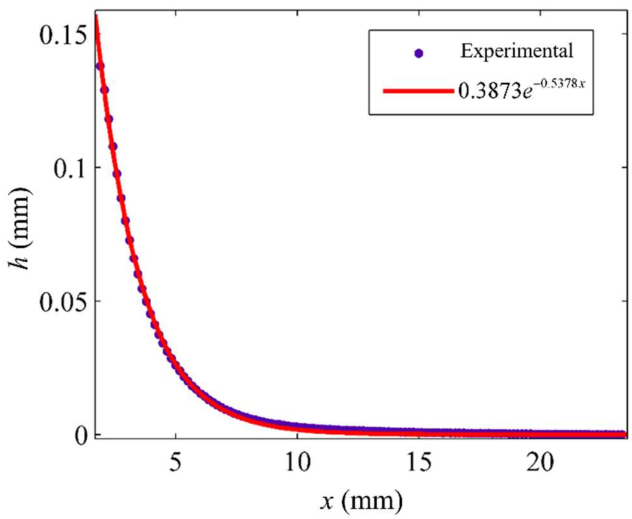

Fig. 7: Experimentally measured meniscus profile and fitted curve.

In summary, Schlieren imaging provides an effective platform for measuring surface tension induced liquid surface deformations. We use ray tracing to show that displacement of the background pattern due to meniscus curvature is directly proportional to surface gradient as long as a correction factor for inclined glass plate is taken into account. In order to validate the technique, we measure meniscus profile over an inclined flat plate for different test liquids, which are then compared with the theoretical expression to extract surface tension and contact angle as fit parameters. The experimentally determined surface tension values were found to be in close agreement with the results obtained from pendant drop technique and the data found in literature. It leads to two key conclusions, 1) surface tension induced meniscus can be reliably measured by Schlieren imaging, and 2) the proposed experimental platform can be used for estimation of surface tension and liquid refractive index. Schlieren imaging could be a valuable alternative to sessile drop or pendant drop methods that are difficult to use for inhomogeneous substrates and low surface tension liquids, respectively.

Even though meniscus for inclined plate case is translationally symmetric, the experimental method does not make that assumption and measures the surface profile over the full contact line in the field of view. This can also be understood from Equation 18, $(\partial h/\partial x)\,\hat{i} + (\partial h/\partial y)\,\hat{j} = -(\boldsymbol{\delta r} - \mathbf{MM^{o}})/\alpha h_p$. An arbitrary surface such as a meniscus between two self-assembling particles would produce comparable background displacement in both the x and y directions. Also, in such cases, a glass plate may not be present between the background pattern and the meniscus. As a result, $\mathbf{MM^{o}}$ can be set to zero. In that sense, Equation 18 presents a more general solution. In future, experimental measurement of surface profile of meniscus can provide insights in the study of various interfacial phenomena[15,16].

Notes and references

[a] Birck Nanotechnology Centre, School of Mechanical Engineering, Purdue University, West Lafayette, IN – 47907

[b] Maurice J. Zucrow Laboratories, School of Mechanical Engineering, Purdue University, West Lafayette, IN – 47907

Electronic Supplementary Information (ESI) available.

1 H.-J. Butt, W. J. P. Barnes, A. del Campo, M. Kappl and F. Schönfeld, *Soft Matter*, 2010, **6**, 5930.
2 M. Zakerin, M. Kappl, E. H. G. Backus, H.-J. Butt and F. Schönfeld, *Soft Matter*, 2013, **9**, 4534.
3 D. Vella, *Annu. Rev. Fluid Mech.*, 2015, **47**, 115–135.
4 D. L. Hu, B. Chan and J. W. M. Bush, *Nature*, 2003, **424**, 663–6.
5 J. Liu, J. D. Paul and J. P. Gollub, *J. Fluid Mech.*, 2006, **250**, 69.
6 K. Sakai, D. Mizuno and K. Takagi, *Phys. Rev. E*, 2001, **63**, 046302.
7 D. Dabiri and M. Gharib, *Exp. Fluids*, 2001, **30**, 381–390.
8 F. Moisy, M. Rabaud and K. Salsac, *Exp. Fluids*, 2009, **46**, 1021–1036.
9 J. Drelich, *Encycl. Surf. Colloid Sci.*, 2002, 3152–3166.
10 D. Y. Kwok, W. Hui, R. Lin and A. W. Neumann, *Langmuir*, 1995, **11**, 2669–2673.
11 M. Raffel, C. E. Willert, S. T. Wereley and J. Kompenhans, *Particle Image Velocimetry: A Practical Guide*, Springer Science & Business Media, 2007.
12 W. M. Haynes, *Handb. Chem. Phys.*, 2012, **93rd editi**, 5–94 – 5–101.
13 A. Goebel and K. Lunkenheimer, *Langmuir*, 1997, **13**, 369–372.
14 G. Vazquez, E. Alvarez and J. M. Navaza, *J. Chem. Eng. Data*, 1995, **40**, 611–614.
15 M. Cavallaro, L. Botto, E. P. Lewandowski, M. Wang and K. J. Stebe, *Proc. Natl. Acad. Sci. U. S. A.*, 2011, **108**, 20923–8.
16 L. Botto, L. Yao, R. L. Leheny and K. J. Stebe, *Soft Matter*, 2012, **8**, 4971.